Belarusian State University
and
Research Center for Public Health (CRP-Sante)

Developing Models, Algorithms, and Software Tools for Simulation and Analysis of Actin Polymerization

Overview of the Subject and Models Developed

Intermediate Report
15.05.2006 – 15.11.2006

Authors:

P.V. Nazarov

A.A. Golovaty

E.A. Barsukov

E.V. Ivashkevich

Supervisors:

Prof. V.V. Apanasovich

Dr. M.M. Yatskou

Prof. E. Friederich

2006

CONTENTS

1. Introduction

Actin polymerization is a complex cell process, involving in cytoskeleton formation, cell movement and division. The study of this process, among pure scientific interest in understanding biophysical principles of cell motility, is motivated by the following reasons:

- several pathogens, like *Listeria monocytogenes*, use actin polymerization for propulsion inside infected cells;
- the motility of cancer cells and metastasis spread is significantly dependent on actin polymerization
- by influencing actin polymerization it is possible to prevent division of cancer cells.

Despite a big number of experimental and theoretical works, related to this subject, the mechanism of force generation as well as a role of crosslinking proteins has not yet been completely understood. The most of the works in this area (except few) are aimed at development of separate phenomenological models, which cannot be used for predictions in a general case. Therefore the main goal of the current study is to develop the computational model, which can be used in a general case to predict the behavior of actin filaments and other objects (beads, bacteria).

This report is a result of intensive literature analysis on actin-related problems. It will outline the subject of research, the experimental studies performed and models developed. In the last section of the report the ideas for the model, which is intended to be developed, are given.

2. Biochemistry overview

Actin polymerization is a rather complex process, involving a number of protein components (see review by Pollard (Pollard and Borisy, 2003)). The main participants of the process are listed in the Table 1, and the model of the biochemical influences is given in Fig 1. Along with the standard "concentration" polymerization (mostly at barbed end), this process can be stimulated by *formin*, which interacts with barbed ends of filaments, speeding up polymerization; *Arp2/3* complex able to nucleate new filaments, producing branching structures (Pollard and Beltzner, 2002); *bundling proteins* can decrease the speed of depolymerization, shifting equilibrium towards elongation of filaments (Loomis et al., 2003).

Table 1. Brief description of the participating proteins

Protein	Description	References
actin	Main building block of actin-filament. Present in two forms G-actin (globular, monomer) and F-actin (filament, polymer). Actin usually is associated with a ATP/ADP molecules, forming 4 subsets of actin population (F-ATP, F-ADP, G-ATP, G-ADP) with different polymerization properties.	All mentioned below
profilin	Performs exchange G(ADP)-actin → G(ATP)-actin.	(Pollard and Borisy, 2003; Romero et al., 2004)
capping	Capping protein inhibits the polymerization by occupation of the free barbed ends of actin filaments	(Pollard and Borisy, 2003; Romero et al., 2004; Vignjevic et al., 2003)
formin	A group of proteins involved in the polymerization of actin. It cooperates in rapidly assembling profilin-actin into long filaments while remaining continuously associated with the fast-growing barbed end.	(Kovar, 2006; Romero et al., 2004)
Arp2/3	Actin-Related Proteins Arp2/3 complex is a seven-subunit protein that serves as nucleation sites for new actin filaments. The complex binds to the sides of existing filaments and initiates growth of a new filament at a distinctive 70°. As a result of this nucleation of new filaments branched actin networks are created.	(Brieher et al., 2004; Giganti et al., 2005; Higgs and Pollard, 1999; Higgs and Pollard, 2001; Pollard and Beltzner, 2002; Sirotkin et al., 2005)

WASP (VCA)	WASP (Wiskott-Aldrich syndrome protein) activates Apr2/3. VCA is the active subunit of WASP.	(Bernheim-Groswasser et al., 2002; Carlier et al., 2003; Giganti et al., 2005; Higgs and Pollard, 1999; Higgs and Pollard, 2001; Loomis et al., 2003; Pollard and Borisy, 2003; Sirotkin et al., 2005; Vignjevic et al., 2003)
ActA	The protein of *L. monocytogenes* induces actin nucleation on the bacterial surface by activation of Arp2/3 and VASP (PRO domain).	(Carlier et al., 2003; DesMarais et al., 2005; Giganti et al., 2005; McGrath et al., 2000; Plastino et al., 2004; Pollard and Borisy, 2003)
VASP	This protein decreases branching of the filaments, at the same time increases the speed of *L. monocytogenes* and beads propulsion. The mechanism is not yet clear. The hypotheses are: VASP detach filaments from ActA complex, or compete with capping proteins	(Plastino et al., 2004; Samarin et al., 2003)
ADF/cofilin	ADF/cofilin is a family of actin-binding proteins that disassembles (severs) actin filaments	(Carlier et al., 2003; Pollard and Borisy, 2003)
fascin	Fascin is an actin-bundling protein and is thought to play a role in the formation of microfilament bundles of microspikes and stress fibers in cultured cells.	(Brieher et al., 2004; Plastino et al., 2004; Tseng et al., 2002; Vignjevic et al., 2003)
espin	Espin is an actin-bundling protein.	(Bartles et al., 1998; Loomis et al., 2003)
fimbrin	Fimbrin is an actin cross-linking protein.	(Giganti et al., 2005; Plastino et al., 2004)
T-plastin L-plastin	Actin cross-linking proteins	(Giganti et al., 2005; Janji et al., 2006)

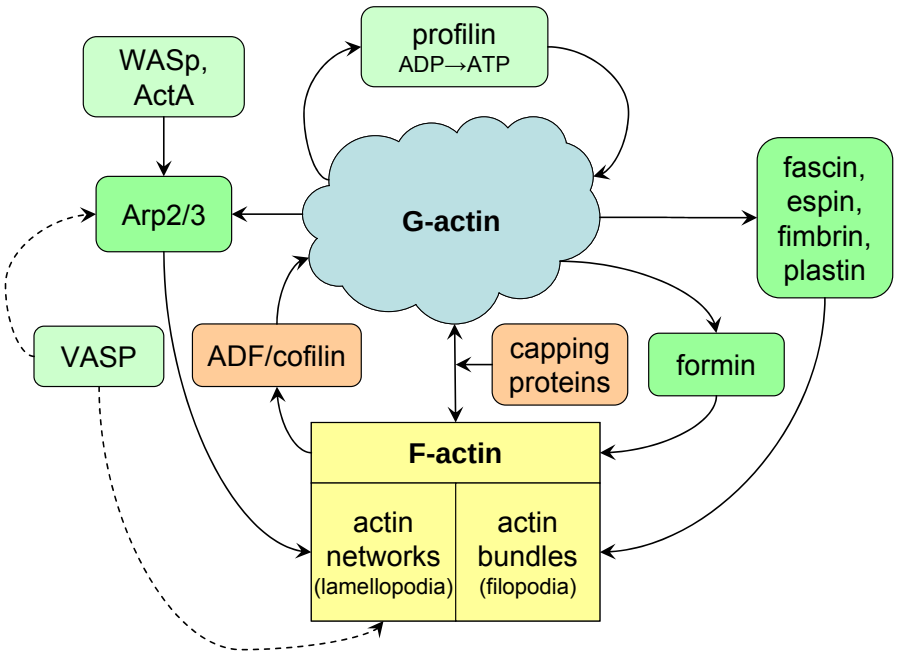

Fig.1. Schematic representation of a simplified biochemical network related to the actin polymerization process.

ADF/cofilin severs filaments. By its actin-severing activity, it creates new actin barbed ends for polymerization and also depolymerizes old actin filaments (Carlsson, 2006; DesMarais et al., 2005). Capping proteins occupy barbed ends, thus preventing polymerization and shifting equilibrium towards depolymerization.

3. Overview of biophysical experiments

One of the first considered experimental works directed to biophysical characterization of the actin polymerization and *L. monocytogenes* motility is (Cameron et al., 1999). Here the behavior of ActA-covered polystyrene bead was analyzed in cytoplasmic extract. Initiation of unidirectional movement of a symmetrically coated particle is a function of bead size and surface protein density. Small beads (<0.5 μm in diameter) initiate actin-based motility when local asymmetries are built up by random fluctuations of actin filament density or by thermal motion. Larger beads (up to 2 μm in diameter) can initiate movement only if surface asymmetry is introduced by coating the beads on one hemisphere. This explains why the relatively large *L. monocytogenes* requires polar distribution of ActA on its surface to move.

In the paper (Noireaux et al., 2000) authors studied similarities and differences in behavior of ActA coated beads and *L. monocytogenes* On ActA-grafted beads F-actin is formed in a spherical manner, whereas on the bacteria a "comet-like" tail of F-actin is produced. They show experimentally that the stationary thickness of the gel depends on the radius of the beads. Moreover, the actin gel is not formed if the ActA surface density is too low. A theoretical model able to explain how the mechanical stress (due to spherical geometry) limits the growth of the actin gel was proposed. The model predicts conditions for developing of actin comet tails.

In (Bernheim-Groswasser et al., 2002) was found that Wiskott Aldrich syndrome protein (WASP) subdomain, known as VCA, is sufficient to induce actin polymerization and movement when grafted on microspheres. Changes in the surface density of VCA protein or in the microsphere diameter markedly affect the velocity regime, shifting from a continuous to a jerky movement resembling that of the mutated 'hopping' *L. monocytogenes*.

A minimum motility medium containing five pure proteins (actin, Arp2/3, ADF/cofilin, profilin, capping proteins) was used in (Carlier et al., 2003) to study the motility of particles of various sizes and geometries (rods, microspheres).

Similar work is performed in (Cameron et al., 2004), where they have systematically varied a series of biophysical parameters and examined their effects on initiation of motility (of beads or *L. monocytogenes*), particle speed, speed variability, and path trajectory. Symmetry breaking and movement initiation occurred by two distinct modes: either stochastic amplification of local variation for small beads in concentrated extracts, or gradual accumulation of strain in the actin gel

for large beads in dilute extracts. Neither mode was sufficient to enable spherical particles to break symmetry in the cytoplasm of living cells.

Interesting experimental study in (Giardini et al., 2003) involved lipid vesicles covered with ActA in cytoplasmic extract, provides direct insight on the forces affecting vesicle surface due to analysis of its deformation. There was a spatial segregation of the pushing and retarding forces, such that pushing predominates along the sides of the vesicle, although retarding forces predominate at the rear. They estimated that the total net (pushing minus retarding) force generated by the actin comet tail is ~0.4–4 nN.

Similar system was used in (Upadhyaya et al., 2003), where they introduced an experimental system in which lipid vesicles coated with the *L. monocytogenes* virulence factor ActA are propelled by actin polymerization. The polymerization forces cause significant deformations of the vesicle. These deformations were used to obtain a spatially resolved measure of the forces exerted on the membrane using a model. Their results indicate that actin exerts retractile or propulsive forces depending on the local membrane curvature and that the membrane is strongly bound to the actin gel.

The work of Samarin et al (Samarin et al., 2003) is devoted to study the influences of VASP protein on the bead movement in a minimum motility medium. VASP increases branch spacing of filaments in the actin tail. The effect of VASP on branch spacing is opposed to the effect of capping proteins, however, VASP does not compete with capping proteins for binding barbed ends of actin filaments. VASP increases the rate of dissociation of the branch junction from immobilized ActA, which is the rate-limiting step in the catalytic cycle of site-directed filament branching.

VASP effects have been studied also in (Plastino et al., 2004). They show that the degree of filament alignment in the actin comet tails depended on the surface ratio of VASP to Arp2/3 activating proteins (PRO and VCA respectively). Alignment of actin filaments parallel to the direction of bead movement in the presence of VASP was accompanied by an abrupt 7-fold increase in velocity that was independent of bead size and by hollowing out of the comets. The actin filament-bundling proteins fimbrin and fascin did not appear to play a role in this transformation.

Giganti et al (Giganti et al., 2005) analyzes the effects of T-plastin/T-fimbrin. T-Plastin increased the velocity of VCA beads 1.5 times, stabilized actin comets and concomitantly displaced cofilin, an actin-depolymerizing protein. T-Plastin also decreased the F-actin disassembly rate and inhibited

cofilin-mediated depolymerization. The bead speed, being a function of T-plastin concentration has a maximum around 1μM.

Considering beads in minimal biomimetic system (van der Gucht et al., 2005) shows that the symmetry breaking is based on the release of elastic energy. The dynamics of this process and the thickness at which it occurs depend on the growth rate and mechanical properties of the actin gel. They explain experimental results with a model based on elasticity theory and fracture mechanics.

(Loomis et al., 2003) is devoted to study actin bundling by espin protein in vivo and in vitro. Espin crosslinks cause pronounced barbed-end elongation and, thereby, make a longer bundle without joining shorter modules.

The filament bundle formation form branched actin network is studied in (Vignjevic et al., 2003). They show that directions of filament barbed end in bundles and branched structures are opposite. They proposed a model for filopodial formation in which actin filaments of a preexisting branched network are elongated by inhibition of capping and subsequently cross-linked into bundles by fascin.

The group of Mitchison demonstrates in (Brieher et al., 2004) that *L. monocytogenes* motility can be separated into an Arp2/3-dependent nucleation phase and an Arp2/3-independent elongation phase. Elongation-based propulsion requires a unique set of biochemical factors, like fascin. The elongation-based reaction generates a hollow cylinder of parallel bundles that attach along the sides of the bacterium. Bacteria move faster in the elongation reaction than in the presence of Arp2/3, and the rate is limited by the concentration of G-actin.

F-actin gels of increasing concentrations (25–300 mM) display in vitro a progressive onset of birefringence due to orientational ordering of actin filaments as reported in (Helfer et al., 2005).

The work of Romero et al (Romero et al., 2004) is devoted to formins – initiators of actin assembly. They demonstrated that the forming's domains accelerates hydrolysis of ATP coupled to profilin-actin polymerization and uses the derived free energy for processive polymerization, increasing 15-fold the rate constant for profilin-actin association to barbed ends. Transitory formin-associated processes are generated by poisoning of the processive cycle by barbed-end capping proteins.

In original work by Marcy (Marcy et al., 2004) the forces generated during actin-based propulsion are directly measurement by micromanipulation. By pulling the actin tail away from the bead at high speed, they estimated the elastic modulus of the gel and measured the force necessary to detach the tail from the bead. By applying a constant force in the range of ~1.7 to 4.3 nN, the force-velocity relation was established.

Experimental results given in (Zicha et al., 2003) (FLAP) suggest the active transport G-actins to barbed ends of growing actin filament network.

4. Overview of developed models

4.1. Models for biochemical processes

The mathematical models for the length distributions of actin filaments under the effects of polymerization/depolymerization, and fragmentation are given in (Edelstein-Keshet and Ermentrout, 1998; Ermentrout and Edelstein-Keshet, 1998).

Sept et al in (Sept and McCammon, 2001) provides information about computer simulations and free energy calculations, aimed to determine the thermodynamics and kinetics of actin nucleation and thus identify a probable nucleation pathway and critical nucleus size. The association kinetics for the formation of each structure are determined through a series of Brownian dynamics simulations. The results indicate that the trimer is the size of the critical nucleus.

Carlsson (Carlsson, 2006) have studied the effects of filament severing on their growth. From one side, the severing of the filaments leads to their dissociation, at the same time it increases the number of barbed ends (and therefore – growth speed). Severing and branching are found to act synergistically.

The model, based on the dendritic-nucleation hypothesis for lamellipodial protrusion is given in (Mogilner and Edelstein-Keshet, 2002). They consider a set of partial differential equations for diffusion and reactions of sequestered actin complexes, nucleation, and growth by polymerization of barbed ends of actin filaments, as well as capping and depolymerization of the filaments. The mechanical aspect of protrusion is based on an elastic polymerization ratchet mechanism. See also later works of Mogliner (Mogilner and Oster, 2003; Mogilner and Rubinstein, 2005).

4.2. Mechanical models

In (van Oudenaarden and Theriot, 1999), the bead movement is considered. They show that small beads coated uniformly with a protein that catalyses actin polymerization are initially surrounded by symmetrical clouds of actin filaments. This symmetry is broken spontaneously, after which the beads undergo directional motion. They developed a stochastic theory, in which each actin filament is modeled as an elastic Brownian ratchet.

The process of actin gel formation around beads is also studied in (Noireaux et al., 2000). They propose a theoretical model to explain how the mechanical stress (due to spherical geometry) limits

the growth of the actin gel. They deduced from the work that the force exerted by the actin gel on the bacteria is of the order of 10 pN.

The mechanical model taking into account pushing and back-drawing forces due to actin polymerization around *L. monocytogenes* is presented in (Gerbal et al., 2000). The model leads to a natural competition between growth from the sides and growth from the back of the bacterium, with different velocities and strengths for each. This competition can lead to the periodic motion observed in a *L. monocytogenes* mutant.

The review by (Tracqui et al., 2004) contains information about different modeling approaches (mechanical models, differential equations, computational simulations). The review contains also information about the cytoskeleton computational simulation.

Simulation of single actin filaments is considered in (Ming et al., 2003). Model provides a theoretical basis set for a description of spontaneously occurring thermal deformations, such as undulations, of the filaments. The computationally synthesized deformational modes, in the very low-frequency regime, are in good agreement with theoretical solutions for long homogeneous elastic rods, which confirmed the usefulness of substructure synthesis method.

Nice works of Mogliner et al (Mogilner and Oster, 2003) and (Mogilner and Rubinstein, 2005) are devoted to theoretical study of lamellipodia and filopodia formation. In (Mogilner and Oster, 2003) they apply "tethered ratchet" model to derive the force-velocity relation for *L. monocytogenes* and discuss relations of their theoretical predictions to experimental measurements. In (Mogilner and Rubinstein, 2005) filament bundling and filopodia propulsion is modeled. The model explains characteristic interfilopodial distance of a few microns as a balance of initiation, lateral drift, and merging of the filopodia. The theory suggests that F-actin barbed ends have to be focused and protected from capping (the capping rate has to decrease one order of magnitude) once every hundred seconds per micron of the leading edge to initiate the observed number of filopodia.

The model for filopodia propulsion and filament aggregation is given in (Atilgan et al., 2006) . They find that a critical number of filaments are needed to generate net filopodial growth. Without external influences, the filopodium can extend indefinitely up to the buckling length of the F-actin bundle. Filopodia also attract each other through distortions of the membrane. Monte Carlo and analytical approaches have been used.

The model of deformation of ActA-covered vesicles is given in (Upadhyaya et al., 2003). They have used these deformations to obtain a spatially resolved measure of the forces exerted on the membrane using a model based on the competition between osmotic pressure and membrane stretching. The results indicate that actin exerts retractile or propulsive forces depending on the local membrane curvature and that the membrane is strongly bound to the actin gel.

4.3. Computer simulation models

Alberts et al (Alberts and Odell, 2004) have been developed a holistic computational model for simulation of *L. monocytogenes* propulsion. They simulated actin polymerization at molecular level and take into account interactions of several types (rigidity, elasticity, Brownian) to simulate microeffects, which filaments has on a bacterium. The model which will be developed in our project will be based on their approach (see section Proposed model), with several modification and enhancements.

Simulation presented in (Berro and Martiel, 2005) gives an idea how to handle concentration gradient. The simulation space was divided into cells with constant concentration and Gillespie algorithm was used to simulate reactions of actin polymerization inside those cells. The simulation was performed in 2D space.

5. Data sources overview

It is intended to extract information about the rate constants and other physical parameters from literature. The approximate list of sources is listed below.

- Rate constants (Sept and McCammon, 2001)
- Rate constants for nucleation, elongation, branch junction formation and VASP binding (Samarin et al., 2003).
- Rate constants, diffusion coefficients, thermal energy, etc (Mogilner and Edelstein-Keshet, 2002).
- Rate constants, forces, "spring" coefficient (Mogilner and Oster, 2003)
- Rate constants, concentrations, forces (Alberts and Odell, 2004)
- All necessary parameters for actin bundling simulation (Mogilner and Rubinstein, 2005)
- Rate constants (Carlsson, 2006)
- Some rate constants (Thoumine et al., 2006)
- Dissociation constants (Sirotkin et al., 2005)
- Forces (Giardini et al., 2003)
- Bead diameter-speed-concentration relations (Cameron et al., 2004)
- Formin-related reaction speeds (Romero et al., 2004)

6. Proposed model

6.1. Molecular level

General ideas. The first level of the proposed model is the level of molecular processes: aggregation and dissociation of molecules, forming of complexes, etc. The idea and "participants" of the simulation are depicted in Fig. 2. All "participants" will be divided in two groups: "physical objects" (filaments, bead or bacterium) and "molecules" (G-actin, Arp2/3, capping proteins etc.). The representatives of the first group will be characterized by coordinates, mass, velocity, and angular moments. "Participants" from the second group will be considered only in terms of quantities and concentrations. The coordinate affixment (in some sense) of the latter will be fulfilled only in the final state of model development (see "concentration gradient" below).

Starting simulation algorithm. As a starting point to the simulation model the classical Gillespie approach will be used (so called "first reaction" modification). Being a very simple in terms of programming, it allows precise characterization of rather complex systems. Its only disadvantage is enormously high time costs. That is why this method will be used here only as an initial point for the work and a reference to validate faster algorithms.

Tau-leap method modification. This modification of Gillespie algorithms allows much faster simulation of chemical reactions. Instead of the simulation of the occurrence time for each reaction, it calculates the number of reactions, which took place during a small time τ. This approach fits better to our case, because we are aimed on incorporation of both molecular and mechanical models into one. Most of the mechanical models are handled by considering interaction in the system during a short time. Another possible approach is a semi-analytical one, where the number of reactions is calculated analytically, but reaction localizations are generated randomly.

Concentration gradient. Taking into account the possible concentration gradients for different molecules in the system is one of the most challenging features of the model. Additional study should be performed on the necessity of this feature, and it will be incorporated into the model only at the latest state of development. There are a number of possible algorithms for concentration gradient handling. One of them – is to divide simulation 3D-space into blocks of almost equal concentration and take into account molecule diffusion from each block to the nearest ones. It should be noted, that this will significantly increase the time costs of simulation.

The overall concentration of substances in the sample should also be taken into account and the diffusion between simulated box and remaining part of the sample has to be calculated.

6.2. Mechanical forces

It is intended to consider 3 types of mechanical forces in the system. First, if physical objects are found to be crossed, they experience repulsive force, that allows separating them during 1 time step. Second, attractive forces, which can exist between proteins on the bead or bacterium surface and newly made filaments, or between filaments linked via bundling protein (simulated as elastic springs with finite durability). Third force of random strength and direction is applied to all bodies of the system after each time step to simulate Brown interactions.

6.3. Final mesoscale model

"Physical objects" of the simulated system will be characterized by their mass, coordinates of mass center, geometrical sizes, velocity, and rotation moments. After each small simulation time step *dt* new positions of all objects should be calculated (based on old coordinates and forces from the previous step) and all forces have to be recalculated. If time step *dt* is sufficiently small, the result of this sequential algorithm will be a plausible mechanical interactions of filaments and a bead (bacterium).

Most challenging point in the model is bundling of the proteins. There are no publications about molecular scale models of this process. We will try to handle this problem using the following simplified algorithm. If two filaments appear to be close together, the virtual bundling protein binding site will be generated. Afterwards, bundling proteins will be randomly placed to binding sites.

7. Biochemical model for simplified reactions

7.1. Abbreviations

To unify the names in routines and increase understanding between team-members, the following abbreviations for different types of molecules was proposed. Each functional molecular subset has its own notation.

ACG – actin in G form
ACF – actin in F form
FIB – filament barbed end
FIP – filament pointed end
ARP – Arp 2/3 (free and activated)
ARF – Arp 2/3 (in filament)
CAP – capping protein (free)
CAF – capping protein (in filament)
ADC – ADF/cofilin
FOP – free forming
FOF – formins, bound to barbed ends

7.2. Model overview

To work out the simulation strategy and test the algorithms it was decided to simplify the considered molecular system (at this initial stage). This simplification significantly reduces the number of reactions; however, it saves all important features of the actin system: (de)polymerization, capping, branching and severing.

The simplifications are introduced by the following assumptions:

- no difference between ATP- and ADP-carrying actins in filament;
- very fast work of profilin (all ADP immediately are replaced by ATP) ;
- simplified nucleation reaction (3 G-actins can give a birth to a new filament);
- All free Arp2/3 are considered to be activated (by Act or other activation protein). Activated Arp2/3 bounds to filament side;
- all concentrations are uniform in the considered volume (constant at each point of the volume at the selected time moment t).

The schematic representation of this simplified model is given in Fig. 2. The model includes 10 types of molecular subsets ("players"), each with their own properties: ACG, ACF, FIB, FIP, ARP, ARF, CAP, CAF, ADC.

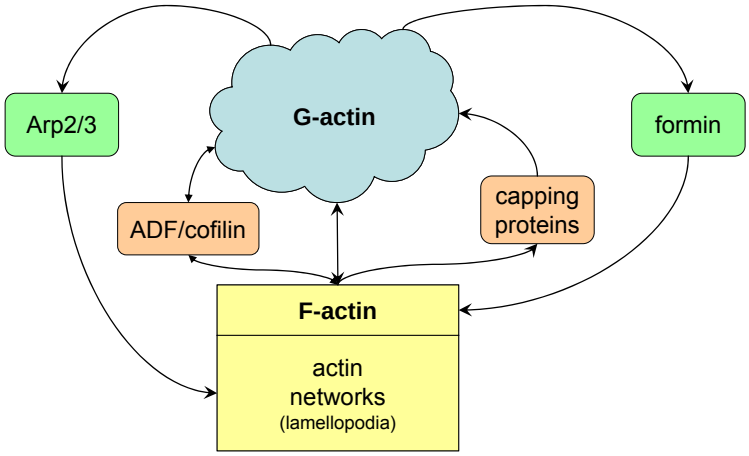

Fig.2. Schematic representation of a simplified biochemical network related to the actin polymerization process.

The reactions, which can be taken into account in the current model, are listed below.

1. Spontaneous nucleation, NUCL — $3ACG \rightarrow 3ACF + FIB + FIP$
2. Nucleation via forming, FNUC — $FOP + 3ACG \rightarrow 3ACG + FIB + FIP + FOF$
3. Association at barbed end, ASSB — $FIB + ACG \rightarrow FIB + ACF$
4. Association at pointed end, ASSP — $FIP + ACG \rightarrow FIP + ACF$
5. Dissociation at barbed end, DISB — $FIB \rightarrow FIB + ACG$
6. Dissociation at pointed end, DISB — $FIP \rightarrow FIP + ACG$
7. Branching, ARPB — $ARP + ACF \rightarrow ARF + ACF + FIP$
8. Capping, CAPB — $CAP + FIB \rightarrow CAF$
9. Severing on the filament, SEVR — $ACF + ADC \rightarrow ACG + ADC + FIP + FIB$
10. Dissolve of short filaments[1], DEPO — $a_1 \cdot ACF + a_2 \cdot ARF + a_3 \cdot CAF + FIB + FIP \rightarrow \rightarrow a_1 \cdot ACG + a_2 \cdot ARP + a_3 \cdot CAP$

7.3. Values of concentrations and rate constants

The standard concentrations used in simulation are listed in Table 2 (the concentrations can vary in different simulations). The values of rate constants given in literature and used in the simplified model are shown in Table 3. Because of the ATP/ADP-neglecting, it is not possible directly use the rate constants for actin (de)polymerization at barbed and pointed ends. Therefore it was decided to

[1] This reaction is not evident. In simulation model it is realized in the following way. If after any action (dissociation, severing and branch detachment) the length of any filament becomes smaller than 2 actins, this filament dissolves.

use limiting values that provides the fast barbed-end polymerization in combination with pointed-end depolymerization (see Table 3 for details).

Table 2. Standard initial concentrations

Molecule	Concentration
ACG	12 μM
ARP	0.3 μM
CAP	1 μM
ADC	3 μM
FOP	~ nM

Table 3. Reaction list and standard reaction rates

Reaction	Rate unit	Rate (*k*) in literature	Reference	Rate (*k*) used
1. *Nucleation* $3 \cdot ACG \rightarrow FIB + FIP + 3 \cdot ACF$	$\mu M^{-2}s^{-1}$	$2.3 \cdot 10^{-11}$	(Samarin et al., 2003)	10^{-6}
2. *Barbed end association* $FIB + ACG \rightarrow FIB + ACF$	$\mu M^{-1}s^{-1}$	11.6 (ATP) 3.8 (ADP)	(Alberts and Odell, 2004)	11.6
3. *Pointed end association* $FIP + ACG \rightarrow FIP + ACF$	$\mu M^{-1}s^{-1}$	1.4 (ATP) 0.16 (ADP)	(Alberts and Odell, 2004)	0.16
4. *Barbed end dissociation* $FIB \rightarrow FIB + AGF$	s^{-1}	1.4 (ATP) 7.2 (ADP)	(Alberts and Odell, 2004)	1.4
5. *Pointed end dissociation* $FIP \rightarrow FIP + AGF$	s^{-1}	0.8 (ATP) 0.27 (ADP)	(Alberts and Odell, 2004)	0.8
6. *Arp2/3 binding* $FIB + ARP \rightarrow ARF$	$\mu M^{-1}s^{-1}$	3.0 ÷ 10.0	(Alberts and Odell, 2004)	3.0
7. *Capping association* $FIB + CAP \rightarrow CAF$	$\mu M^{-1}s^{-1}$	3.0	(Alberts and Odell, 2004)	3.0
8. *Severing* $ACF \rightarrow ACG+FIB+FIP$	$\mu M^{-1}s^{-1}$	$2.3 \cdot 10^{-6}$ s^{-1}	(Carlsson, 2006)	10^{-2}

7.4. Simulation algorithms

Three algorithms of reaction simulation were considered: Gillespie first reaction, τ-leap and modified first reaction algorithm for discrete time. All of them are based on calculation of concentration-dependent rates a_i, such, that the product $a_i dt$ gives the probability for *i*-th reaction to occur in the infinitesimal time *dt*. These rates can be obtained from experimental rate constants *k* using equations, which varies for different types of reactions (Gillespie, 1977). As was calculated for the considered model, these equations are (see reaction numbers in the Table 3):

Reaction 1: $$a_i = k_i \cdot n_I \cdot (n_I - 1) \cdot (n_I - 2) \cdot V^{-2} \cdot N_A^{-2} \cdot 10^{12}$$

Reactions 2, 3, 6, 7: $a_i = k_i \cdot n_I \cdot n_{II} \cdot V^{-1} \cdot N_A^{-1} \cdot 10^6$

Reactions 4, 5: $a_i = k_i \cdot n_I$

In this equations $n_{I,II}$ – number of molecules of types *I* and *II*, V – considered volume in liters, N_A – Avogadro number, k_i has the dimensionality mentioned in Table 3.

Gillespie first reaction. This algorithm is the basic for exact reaction simulation in the case of small amount of well-mixed reacting molecules. Its drawbacks are:

- the algorithm is concerned with the high computational costs, if the number of molecules is high (10^4–10^6)
- the generation of the reaction time does not allow to use this method in the case of discrete time simulation (for instance, in the simulation of mechanical movements, where the time of the system is divided in the set of small times *dt*)

During simulation the time for each *i*-th reaction is calculated as $t_i = -a_i^{-1} \log(\xi)$, where ξ is a random number, uniformly distributed in the interval (0,1). The reaction with the smallest time occurs.

Approximate τ-leap method. This method is a fast approximation of the original Gillespie algorithm. Let us select such a small period of time Δt, that the concentration of each reagent can be considered as a constant during this Δt. During simulation the number of events of each reaction occurrence is calculated and this number of reaction is performed. The flow of events for each reaction is considered as Poisson, therefore the number of i-th reactions during Δt is $N_i(\Delta t) = a_i \Delta t \pm \sqrt{a_i \Delta t}$ (here the standard deviation is given after "±" sign). The performed numerical experiments showed, that applicability of τ-leap method is questionable. If the selected Δt is small, the algorithm does not significantly speed up the simulation (in comparison with "first reaction" method). At the same time, the increase of Δt can lead to instabilities and negative concentrations. Therefore it was decided to omit τ-leap algorithm.

Modified first reaction. It was decided to modify the Gillespie first reaction approach and include into it the events of systems mechanics recalculation as an additional "reaction". The modified approach combines the advantages of first reaction method with discrete-time mechanics recalculation. The idea of the method is introducing 2 parallel times: for reactions (t_{react}) and for mechanics (t_{mech}). The second one had small constant increment Δt, which is supposed to be much smaller then average discrete on reaction time: $\Delta t << mean(t_{react}^{i+1} - t_{react}^{i})$. After each reaction a

number of mechanical movements are performed with discreet time t_{mech} until $t_{mech}>t_{react}$. Then algorithm simulates the next reaction.

7.5. Simulation program

In the simulation model for biochemical reactions each filament is characterized only by the numbers of F-actins (ACF), bound capping proteins (CAF) and bound Arp2/3 (ARF). The precise structure of the filament is unknown. However, the knowledge about the number of proteins in each filament is sufficient for Monte Carlo simulation of filament behavior during (de)polymerization. The model was realized as a part of software tool ActinSimChem. The screenshot of the developed program is given in Fig. 3.

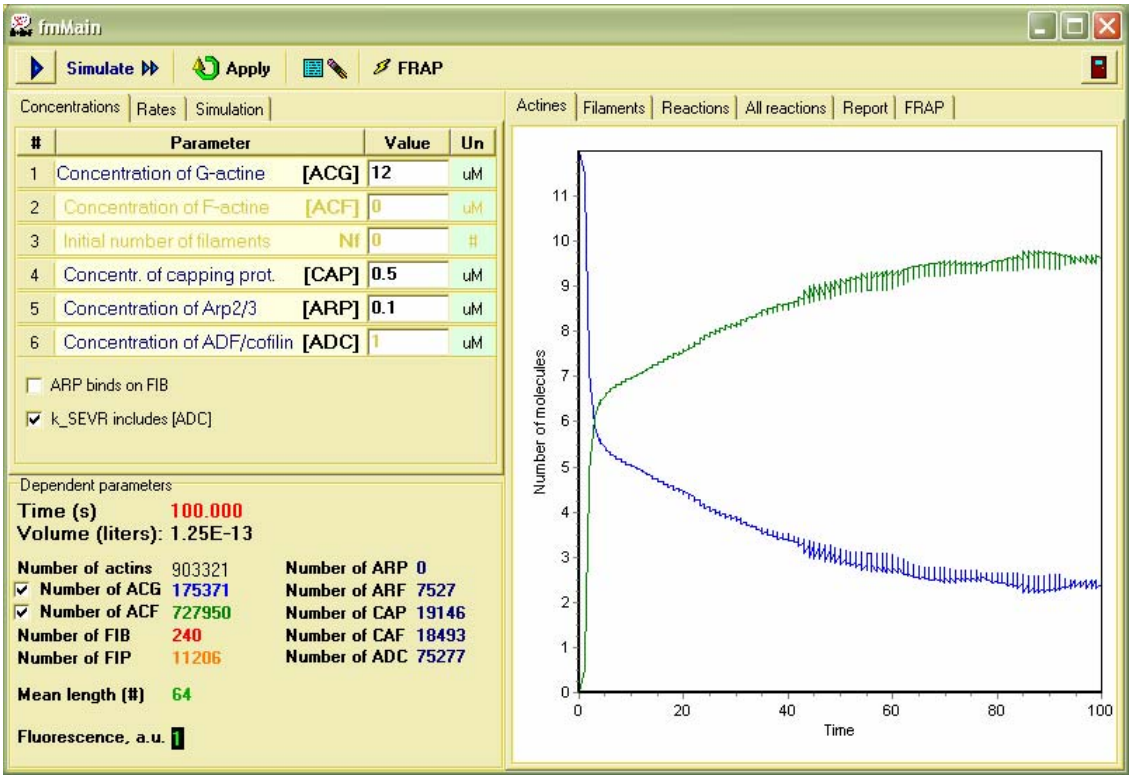

Fig. 3. Screenshot of ActinSimChem with the results of several simulations of the actin polymerization. Blue line – G-actin, green – F-actin. Time is given in seconds.

7.6. Developing of the analytical model for the simplified reactions

Consider "minimal" actin-polymerization system, including G-, F-actins, Arp2/3, capping and severing proteins. The concentration of severing protein let's consider constant, and the time of the interaction of severing protein with a filament very small. With this assumptions the system can be described with 8 "players" (ACG, ACF, FIB, FIP, ARP, ARF, CAP, CAF) and 6 reactions

(nucleation FORM, association at barbed end ASSB, dissociation at pointed DISP, branching ARPB, capping CAPB, severing SEVR). As a non-evident 7th reaction the complete dissociation of short filaments (with length of <3 actins) can be considered.

There are two ways for the analytical description of this system. In the first approach the number of dissolved filaments (denote as X) is estimated by the product of $k_{DEPO} \cdot FIP$. The value of the depolymerization rate k_{DEPO} and average length of depolymerized filaments a are found from simulation model.

$$
\begin{aligned}
&\frac{\partial ACG}{\partial t} = -3 \cdot k_{FORM} \cdot ACG^3 - k_{ASSB} \cdot ACG \cdot FIB - k_{ASSP} \cdot ACG \cdot FIP + \\
&+ k_{DISB}\left(1 - \frac{ARF}{ARF + ACF}\right) FIB + k_{DISP} \cdot FIP + k_{SEVR} \cdot ACF \cdot ADC + a \cdot X(\partial t) \\
&\frac{\partial ACF}{\partial t} = -\frac{\partial ACG}{\partial t} \\
&\frac{\partial FIB}{\partial t} = k_{FORM} \cdot ACG^3 + k_{SEVR} \cdot ACF \cdot ADC + k_{ARPB} \cdot ARP \cdot FIB - k_{CAPB} \cdot CAP \cdot FIB - \\
&- \left(1 - \left(1 + a\frac{ARF}{ACF}\right)\frac{CAF}{FIP + ARF} + a\frac{ARF}{ACF}\right) X(\partial t) \\
&\frac{\partial FIP}{\partial t} = k_{FORM} \cdot ACG^3 + k_{SEVR} \cdot ACF \cdot ADC + k_{DISP}\left(\frac{ARF}{ARF + ACF}\right) FIP - X(\partial t) \\
&\frac{\partial ARP}{\partial t} = k_{DISP}\left(\frac{ARF}{ARF + ACF}\right) FIP - k_{ARPB} \cdot ARP \cdot FIB + a\frac{ARF}{ACF} X(\partial t) \\
&\frac{\partial ARF}{\partial t} = -\frac{\partial ARP}{\partial t} \\
&\frac{\partial CAP}{\partial t} = -k_{CAPB} \cdot CAP \cdot FIB + \left(1 + a\frac{ARF}{ACF}\right)\frac{CAF}{FIP + ARF} X(\partial t) \\
&\frac{\partial CAF}{\partial t} = -\frac{\partial CAP}{\partial t}
\end{aligned}
\qquad (1)
$$

However, this approach leaded to deviations between simulation and analytical modeling for long times. Therefore the second approach was developed and used. In this approach all different events, which can lead to depolymerization of short filaments are treated separately. The only empirical parameter, that is used in this approach, is the probability for the filament to have the smallest length (3 actins) $p_{=3}$, which should be defined from simulation.

To write down the system of differential equations it was assumed that:

- Short filaments (length < 3) can appear only as a result of severing or dissociation.
- Severing: we consider, that when ADF/cofilin severs the filament near filaments, new short filaments do not appear. F-actins of the short part directly go to G-actin pool.
- Dissociation: the item for actins which go to G-actin pool during dissociation is:

$$k_{DIS} \cdot end \cdot \left(3 \cdot p_{=3} + p_{>3}\right) = k_{DIS} \cdot end \cdot \left(1 + 2 \cdot p_{=3}\right) \tag{2}$$

where k_{DIS} – one of the dissociation speeds;

end – concentration of the corresponding filament ends;

$p_{=3}$ – probability, that the length of a filament at current moment of time is 3;

$p_{>3}$ – probability, that the length of a filament at current moment of time is >3

The full system of differential equations for 8 "players" is

$$\begin{cases} \dfrac{\partial ACG}{\partial t} = -3 \cdot k_{FORM} \cdot ACG^3 - k_{ASSB} \cdot ACG \cdot FIB + k_{DISP} \cdot FIP\left(1 + 2 \cdot p_{=3}\right) + k_{SEVR} \cdot ACF\left(1 + \dfrac{3}{l} + \dfrac{3}{l_b}\right) \\ \dfrac{\partial ACF}{\partial t} = -\dfrac{\partial ACG}{\partial t} \\ \dfrac{\partial FIB}{\partial t} = k_{FORM} \cdot ACG^3 + k_{SEVR} \cdot ACF\left(1 - \dfrac{3}{l}\left(1 - \dfrac{ARF}{ACF}\right) - \dfrac{3}{l_b} \cdot \dfrac{FIB}{FIP + ARF}\left(1 - \dfrac{ARF}{ACF}\right)\right) + \\ \qquad + k_{ARPB} \cdot ARP \cdot ACF - k_{CAPB} \cdot CAP \cdot FIB - k_{DISP} \cdot FIP \cdot \left(1 + 3 \cdot \dfrac{ARF}{ACF}\right) \cdot \dfrac{FIB}{FIP + ARF} \cdot p_{=3} \\ \dfrac{\partial FIP}{\partial t} = k_{FORM} \cdot ACG^3 + k_{SEVR} \cdot ACF\left(1 - \dfrac{1}{l}\left(3 - 6\dfrac{ARF}{ACF}\right) - \dfrac{1}{l_b}\left(3 - 6\dfrac{ARF}{ACF}\right)\right) - k_{DISP} \cdot FIP \cdot p_{=3} \\ \dfrac{\partial ARP}{\partial t} = -k_{ARPB} \cdot ARP \cdot ACF + k_{SEVR} \cdot ACF\left(\dfrac{3}{l}\dfrac{ARF}{ACF} + \dfrac{3}{l_b}\dfrac{ARF}{ACF}\right) + k_{DISP} \cdot FIP \cdot 3\dfrac{ARF}{ACF} \cdot p_{=3} \\ \dfrac{\partial ARF}{\partial t} = -\dfrac{\partial ARP}{\partial t} \\ \dfrac{\partial CAP}{\partial t} = -k_{CAPB} \cdot CAP \cdot FIB + k_{SEVR} \cdot ACF \cdot 3\dfrac{CAF}{ACF}\left(1 - \dfrac{ARF}{ACF}\right) + \\ \qquad + k_{DISP} \cdot FIP \cdot \left(1 + 3 \cdot \dfrac{ARF}{ACF}\right) \cdot \dfrac{CAF}{FIP + ARF} \cdot p_{=3} \\ \dfrac{\partial CAF}{\partial t} = -\dfrac{\partial CAP}{\partial t} \end{cases} \tag{3}$$

Using the known relation between FIB, FIP, ARF, CAF

$$FIB = FIP + ARF - CAF, \tag{4}$$

initial concentrations of actins, Arp2/3 and capping proteins (A, R and C respectively)

$$ACF = A - ACG \tag{5a}$$

$$ARP = R - ARF \tag{5b}$$

$$CAP = C - CAF \tag{5c}$$

and denoting l – average length of the filament, l_b – average length of a branch,

$$l = (A - ACG) / FIP \tag{6a}$$

$$l_b = (A - ACG) / (FIP + AFR) \tag{6b}$$

the system (2) can be simplified into the system of four linearly independent equations.

$$\begin{cases} \dfrac{\partial ACG}{\partial t} = -3 \cdot k_{FORM} \cdot ACG^3 - k_{ASSB} \cdot ACG \cdot (FIP + ARF - CAF) + k_{DISP} \cdot FIP(1 + 2 \cdot p_{=3}) + \\ \qquad + k_{SEVR} \cdot (A - ACG)\left(1 + \dfrac{3}{l} + \dfrac{3}{l_b}\right) \\ \dfrac{\partial FIP}{\partial t} = k_{FORM} \cdot ACG^3 + k_{SEVR} \cdot (A - ACG)\left(1 - \dfrac{1}{l}\left(3 - 6\dfrac{ARF}{A - ACG}\right) - \dfrac{1}{l_b}\left(3 - 6\dfrac{ARF}{A - ACG}\right)\right) - \\ \qquad - k_{DISP} \cdot FIP \cdot p_{=3} \\ \dfrac{\partial ARF}{\partial t} = k_{ARPB} \cdot (R - ARF) \cdot (A - ACG) - k_{SEVR} \cdot (A - ACG)\left(\dfrac{3}{l}\dfrac{ARF}{A - ACG} + \dfrac{3}{l_b}\dfrac{ARF}{A - ACG}\right) - \\ \qquad - k_{DISP} \cdot FIP \cdot 3\dfrac{ARF}{A - ACG} \cdot p_{=3} \\ \dfrac{\partial CAF}{\partial t} = k_{CAPB} \cdot (C - CAF) \cdot (FIP + ARF - CAF) - k_{SEVR} \cdot (A - ACG) \cdot 3\dfrac{CAF}{A - ACG}\left(1 - \dfrac{ARF}{A - ACG}\right) - \\ \qquad - k_{DISP} \cdot FIP \cdot \left(1 + 3 \cdot \dfrac{ARF}{A - ACG}\right) \cdot \dfrac{CAF}{FIP + ARF} \cdot p_{=3} \end{cases} \tag{7}$$

7.7. Comparison of the analytical and simulation models for the simplified reactions

The simulation results were compared with the results of simulation modeling. One of the examples of numerical experiment is presented below.

Initial concentrations: A = 12 μM, R = 0.1 μM, C = 1 μM.

Rate constants:

$$k_{FORM} = 1 \cdot 10^{-6} \mu M^{-2} s^{-1}$$

$$k_{ASSB} = 10 \mu M^{-1} s^{-1}$$

$$k_{DISP} = 0.6 s^{-1}$$

$$k_{CABP} = 3 \mu M^{-1} s^{-1}$$

$$k_{SEVR} = 2.3 \cdot 10^{-6} s^{-1}$$

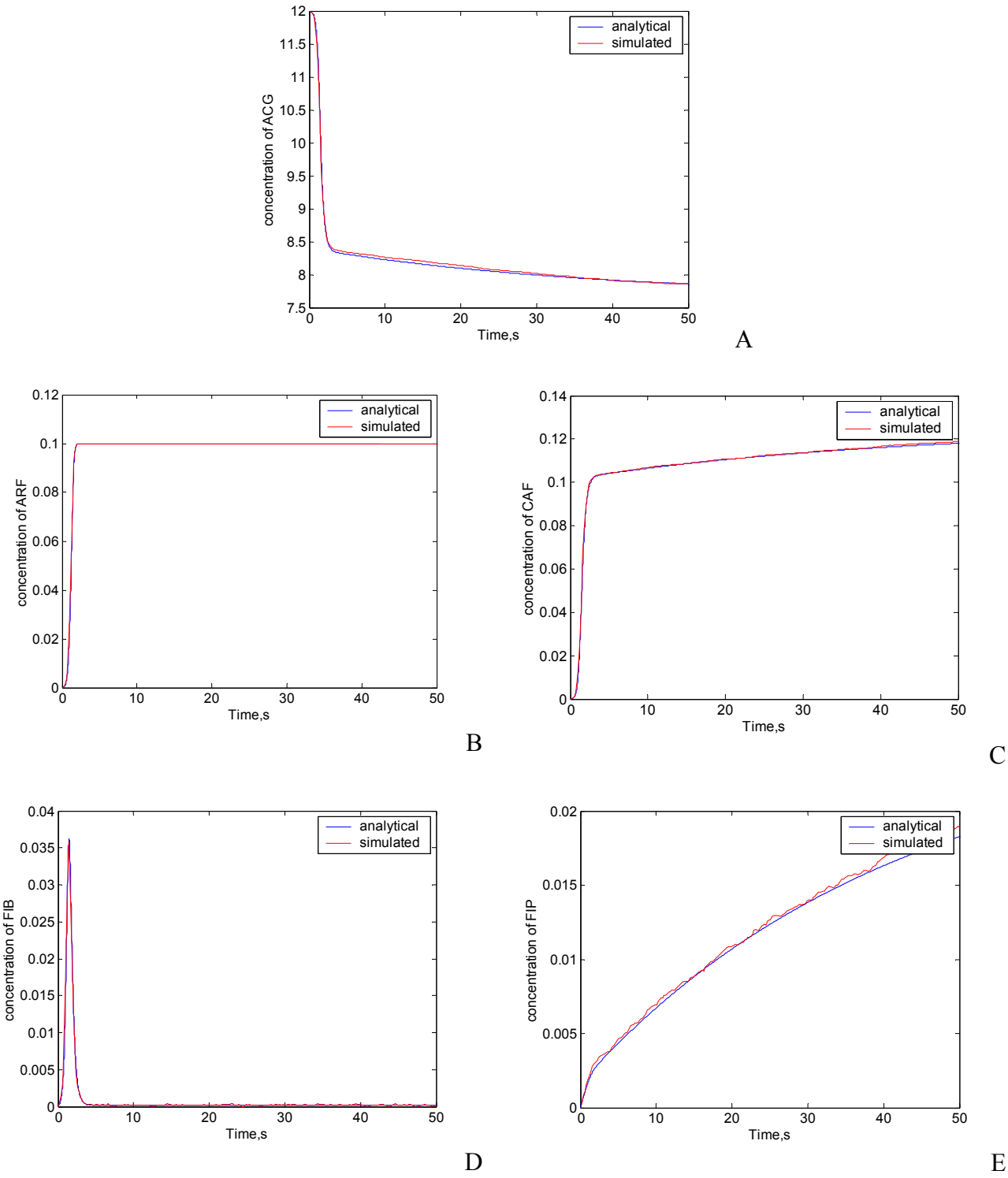

Fig.4. Comparison of the modeling results: blue line – analytical modeling, red line – simulation.

It can be seen, that the behaviors of two models are perfectly in agreement.

Two stages can be seen for this particular numerical experiment from the concentration dynamics. The first is characterized by rapid filament growth just after first filament nucleation. The reason is in fast attachment of free Arp2/3 (we suppose that all free Arp2/3 are activated) to the new filament,

producing more barbed ends and so – increasing the speed of filament formation. After the pool of free Arp2/3 is empty, the second stage of dynamics begins. Free barbed ends are almost completely capped by capping proteins (see their behavior in Fig. 4D) and the filament growth is almost completely dependent barbed ends which appear after severing. These factors lead to the smooth filament growth, starting approximately after 4 seconds after initial nucleation (Fig.4A).

8. Mesoscale 3D model of actin filament system

8.1. Hierarchy of the models

To be able to simulate bead and bacteria propulsion it was decided to imitate the small volume of 3D-space filled with solution of proteins, filaments and small physical bodies. This mesoscale model is base on two main blocks (see Fig. 5): the model for molecular reactions and forces, representing mechanical interactions. In this model filaments and a bead (bacterium) are considered as physical objects, described by their coordinates, masses, velocities, inertia tensors, etc. Free proteins are considered in terms of concentrations. For the moment it was decided to assume constant protein concentrations in the considered volume. In future the volume can be divided into smaller sub-volumes and the gradients of concentrations could be taken into account.

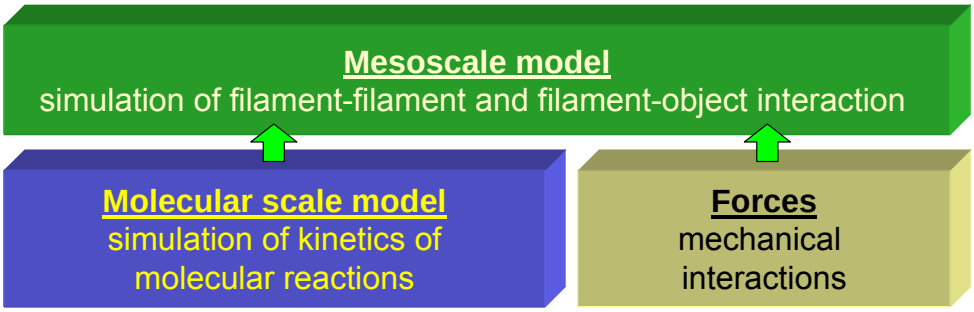

Fig.5. Hierarchy of the mesoscale model.

The model for reactions has been described in details in section 7.4 (modified Gillespie's "first reaction" method). Consider now the structural representations of the filaments (in terms of C++ classes) and the mechanical model for filament motility.

8.2. C++ class for branched actin filament representation

To describe the simulated volume, filaments and mechanical interactions the set of C++ classes was developed. The classes and their hierarchy are shown in Fig. 6.

Class CFilament contains the coordinates of the barbed end and pointed end and the list of children-filaments, which are attached to it (branches). This hierarchic representation allows simple description of all possible tree-form filaments by a single class.

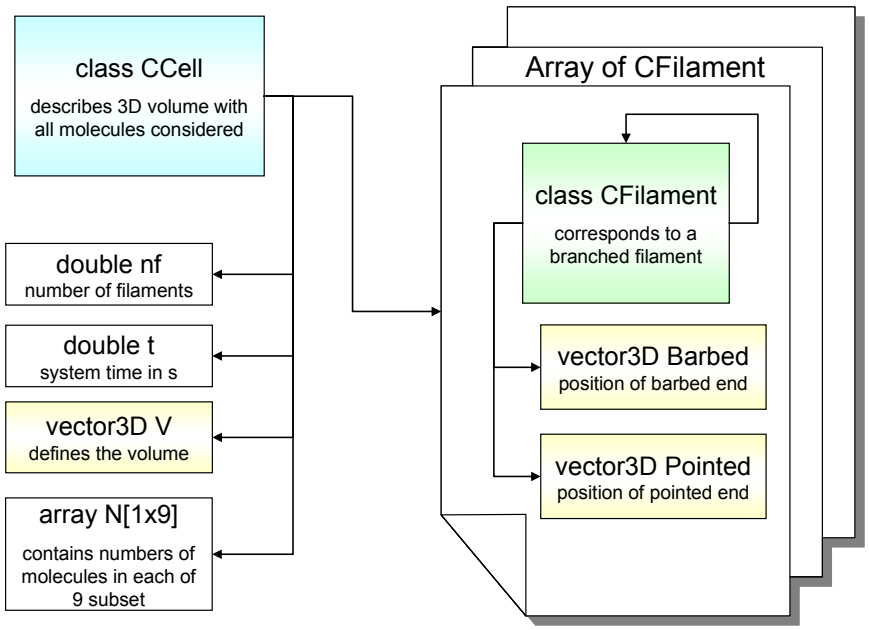

Fig. 6. Developed C++ classes. Colors represent objects (classes).

To visualize the 3D structures, the OpenGL based visual component for Borland C++ Builder was developed. The component allows to draw a number of graphic primitives: points, lines, spheres, cylinders, etc. The example of the branched filament representation is shown in the Fig. 7.

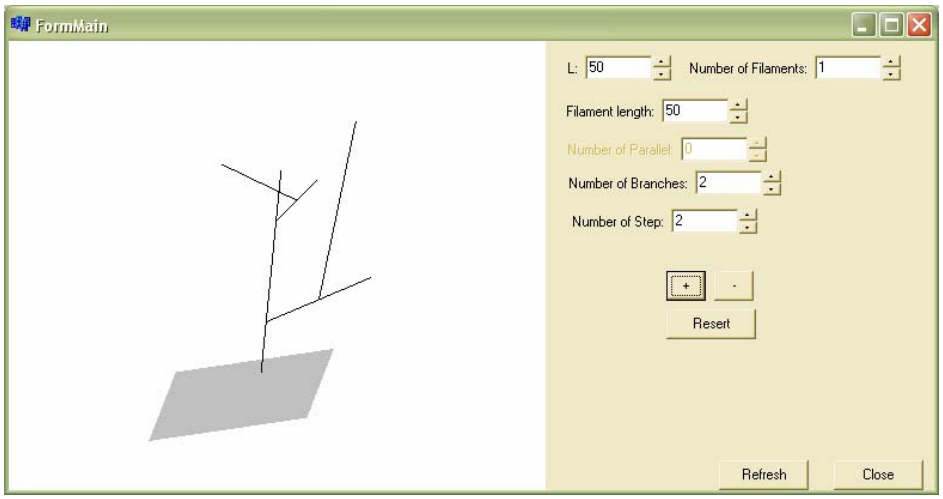

Fig.7. Schematic representation of a simplified biochemical network related to the actin polymerization process.

8.3. *Mechanical model*

For the description of the filament suspension as a mechanical system the classical Newton approach was used. Filaments are considered as solid bodies, made of rigidly bound rods. Two coordinate systems are used to describe the motions of the solid body: fixed (inertial) and mobile, bound to the point of origin in the inertia center of the body.

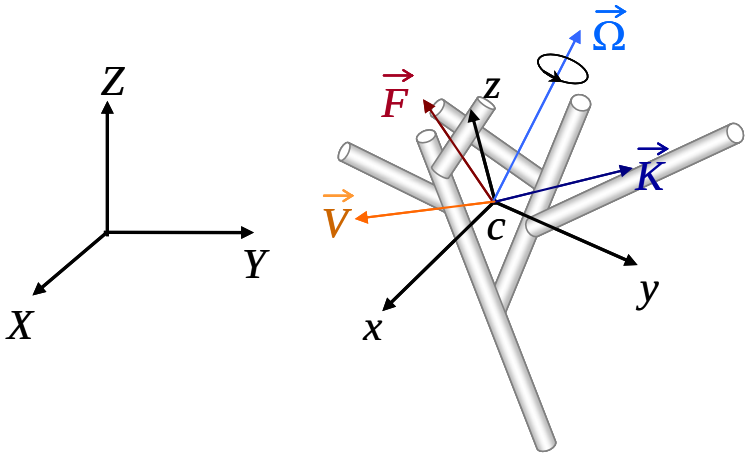

Fig.8. Fixed coordinate system (*XYZ*) and a filament with center of mass *c* and its own mobile coordinate system (*xyz*). Several moment vectors characterizing its behavior are depicted: *F* – net force, *K* – impulse moment, *V* – translational velocity, Ω – rotational velocity.

The equations for the translational and rotational motions can be obtained via integration of the second Newton law.

Translational motion. The second Newton law for translational motion is:

$$\begin{aligned} \vec{a}_c &= \vec{F}/m \\ \vec{a}_c &= d\vec{V}_c/dt \\ \vec{V}_c &= d\vec{R}_c/dt \end{aligned} \tag{8}$$

where

$\vec{a}_c$ – linear acceleration of the mass center *c*;

$\vec{V}_c$ – linear velocity of the mass center *c*;

$\vec{R}_c$ – radius-vector of the mass center *c*;

$\vec{F}$ – net force;

m –mass of the filament;

By integration of (8) using finite difference method the low of translational motion during short time Δ_t can be obtain

$$\begin{aligned} \vec{R}_c(t+\Delta_t) &= \vec{R}_c(t) + \vec{V}_c(t)\Delta_t + \Delta\vec{V}_c/2 \\ \vec{V}_c(t+\Delta_t) &= \vec{V}_c(t) + \Delta\vec{V}_c \\ \Delta\vec{V}_c &= \vec{F}\Delta_t/m \end{aligned} \tag{9}$$

Rotational motion. The second Newton law for rotational motion is:

$$\begin{aligned} &\frac{d\vec{M}}{dt} + \left[\vec{\Omega} \times \vec{M}\right] = \vec{K} \\ &\vec{M} = \mathbf{I}\vec{\Omega} \\ &\vec{\Omega} = \frac{d\vec{\varphi}}{dt} \end{aligned} \quad , \tag{10}$$

where

$\vec{M}$ – moment of the impulse of a solid body;

$\vec{K}$ – moment of the net force, determined respectively mass center;

$\vec{\Omega}$ – angular velocity;

I – inertia tensor of the filament;

$\vec{\varphi}$ – vector of the rotation angle respectively to the mass center.

All this parameters are determined for the filament coordinate system (*xyz*). As for the previouse case, the low of rotational motion during short time Δ_t can be obtained by integration of (10) using finite difference method.

$$\begin{aligned} &\vec{\varphi}(t+\Delta_t) = \vec{\varphi}(t) + \vec{\Omega}(t)\Delta_t + \Delta\vec{\Omega}\Delta_t/2 \\ &\vec{\Omega}(t+\Delta_t) = \vec{\Omega}(t) + \Delta\vec{\Omega} \\ &\Delta\vec{\Omega} = \mathbf{I}^{-1}\left(\vec{K} - \left[\vec{\Omega}(t) \times \left(\mathbf{I}\vec{\Omega}(t)\right)\right]\right)\Delta_t \end{aligned} \tag{11}$$

The general form for the inertia tensor **I** is defined as

$$\mathrm{I}_{ik} = \int \rho_V \left(x_j x_i \delta_{ik} - x_i x_k\right) dV, \quad i, j, k = 1..3 \tag{12}$$

where ρ_V – cubic density.

From Eq. 12 it is obviously, that for the filament containing *n* rods the inertia tensor can be calculated as a sum of inertia tensors of rods ($\mathbf{I}_j$):

$$\mathbf{I} = \sum_{j=1}^{n} \mathbf{I}_j \tag{13}$$

Because the inertia tensor is defined in filament own coordinate system (*xyz*), it stays constant for each filament during motions, while filament shape stays unchanged.

Let us consider the rods, which represent actin-filaments, as cylinders with radius r_0 and some length L_j (for *j*-th rod). Inertia tensor of such cylinder (assuming that its main axis is collinear to *z* axis of its internal coordinate system *C'*, and mass center is located at the origin of this axis system) can be written in the form

$$\mathbf{I}_{jC'} = \begin{bmatrix} m_j\left(r_0^{\,2} + L_j^{\,2}/3\right)/4 & 0 & 0 \\ 0 & m_j\left(r_0^{\,2} + L_j^{\,2}/3\right)/4 & 0 \\ 0 & 0 & m_j r_0^{\,2}/2 \end{bmatrix}, \tag{14}$$

where m_j – mass of the j-th cylinder.

In Eq. 13 the summation is performed in the coordinate system of the entire filament (let us denote it C). Hence, Eq. 14 should be transformed from the cylinder related coordinate system C', to filament-related C. For this the axis system should be sequentially rotated by the angle $\Xi = \left\langle \left(\vec{R}_C - \vec{R}_{1C}\right), (CZ) \right\rangle$, around $C'Y'$, and than by angle $\varphi = \left\langle \left(\vec{R}_C - \vec{R}_{1C}\right)_x, (CX) \right\rangle$ around CZ (see Fig. 9.).

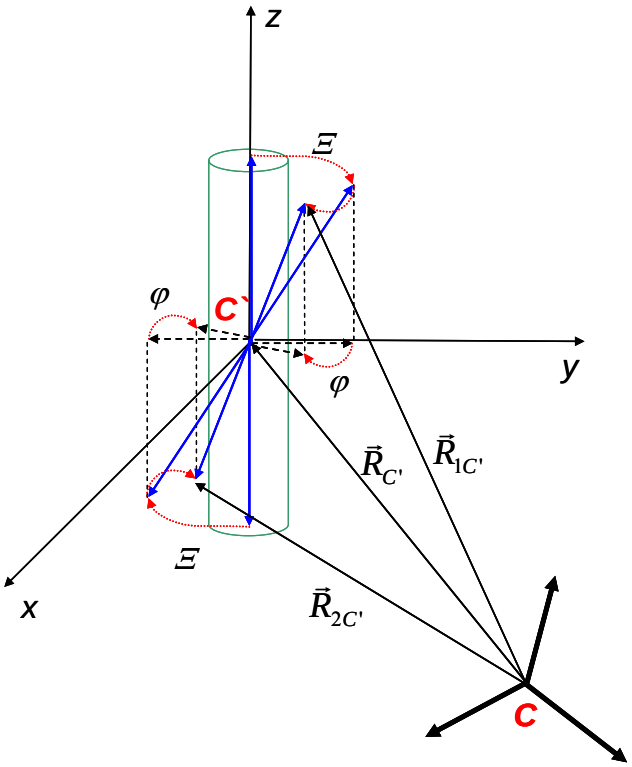

Fig.9. Sequential rotation of the coordinate system C', linked to cylinder.

If such rotations are applied to inertia tensor in C' system, we will get the tensor $\mathbf{I}^{\backslash\backslash}$ in the coordinate system with axes parallel to axes of C, and origin of coordinate shifted by $\vec{R}_C$. To remove the shift, one of the properties of inertia tensor should be used (this property can be derived from definition Eq. 12):

$$\mathrm{I}_{jk} = \mathrm{I}^{//}_{jk} + m_j\left(\left(\vec{R}_{C'}\right)_j\left(\vec{R}_{C'}\right)_k - \left(\vec{R}_{C'}\right)^2 \delta_{jk}\right) \tag{15}$$

Using Eqs. 13 and 15 the tensor for the entire filament can be obtained and used in Eq. 11.

8.4. Considered forces

Forces in the model can be applied to physical objects, including filaments and beads. Four types of forces were suggested to describe interactions of objects between themselves and the medium. These types are (see Fig. 10):

1) Viscous friction of the objects in the media (water). This force is calculated based on the velocities of its parts (~V_c and ~Ω).
2) Repulsion force due to crossing. The value is proportional to the crossing volume and the force is directed normally to the surface of the object.
3) Brownian force with random modulus and momentum, applied to the body after each time discrete Δ_t.
4) Elastic retraction force with finite durability, which simulates molecular linkage. If the force is higher then durability value – the linkage breaks. (*This force is not yet realized in the current model*)

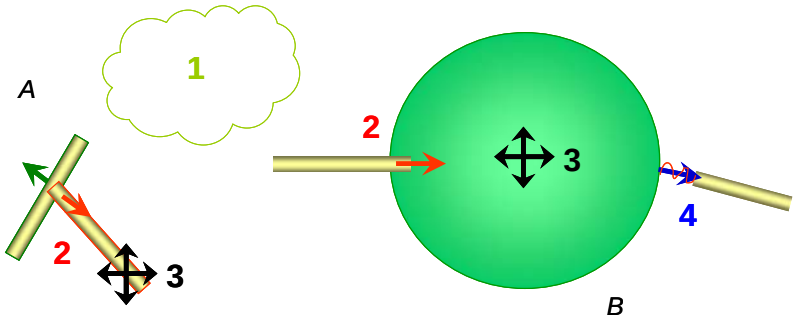

Fig. 10. Types of forces which are considered for filaments-filament (A) and filament-bead (B) interactions.
1 – viscous friction of the medium, 2 – repulsion forces due to crossing of objects,
3 – Brownian forces, 4 – elastic retraction forces simulating molecular linkage.

8.5. Resulted mesoscale model and software tool

The resulted mesoscale model has been realized as a software tool ActinSim3D. The sources has been developed in Borland C++ Builder 6.0. To visualize the simulated 3D volume the free OpenGL package was used. See the screenshot of the software in Fig. 11.

The tasks, performed by this software, are:

1) Monte Carlo simulation of chemical reactions related to actin polymerization
2) Modeling of spatial structure of filaments and their positions
3) Simulation of the filament-filament and filament-bead interactions using Newton dynamics.

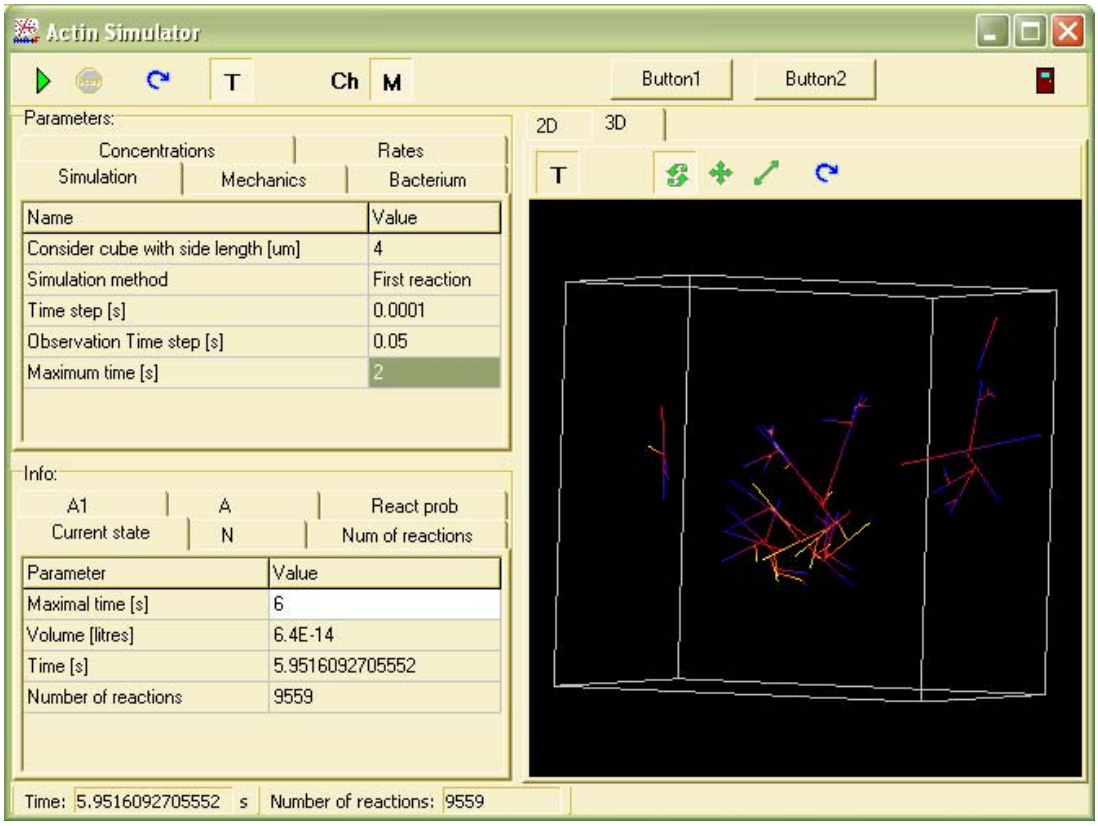

Fig. 11. ActinSim3D software tool with the parameters of simulation in the left window and simulated 3D branced filament structure in the right.

To be able to simulate the nucleation of the filaments on the surface of the bead, the following simplified model was proposed. It was assumed that the rate of nucleation (k_{FORM}) is 100 times higher in the small spherical layer around the bead. This lead to fast nucleation and growth of filament in the close proximity to the bead, forming a actin gel layer around it. Fig. 12 illustrates the time evolution of the polymerization and the resulted bead propulsion.

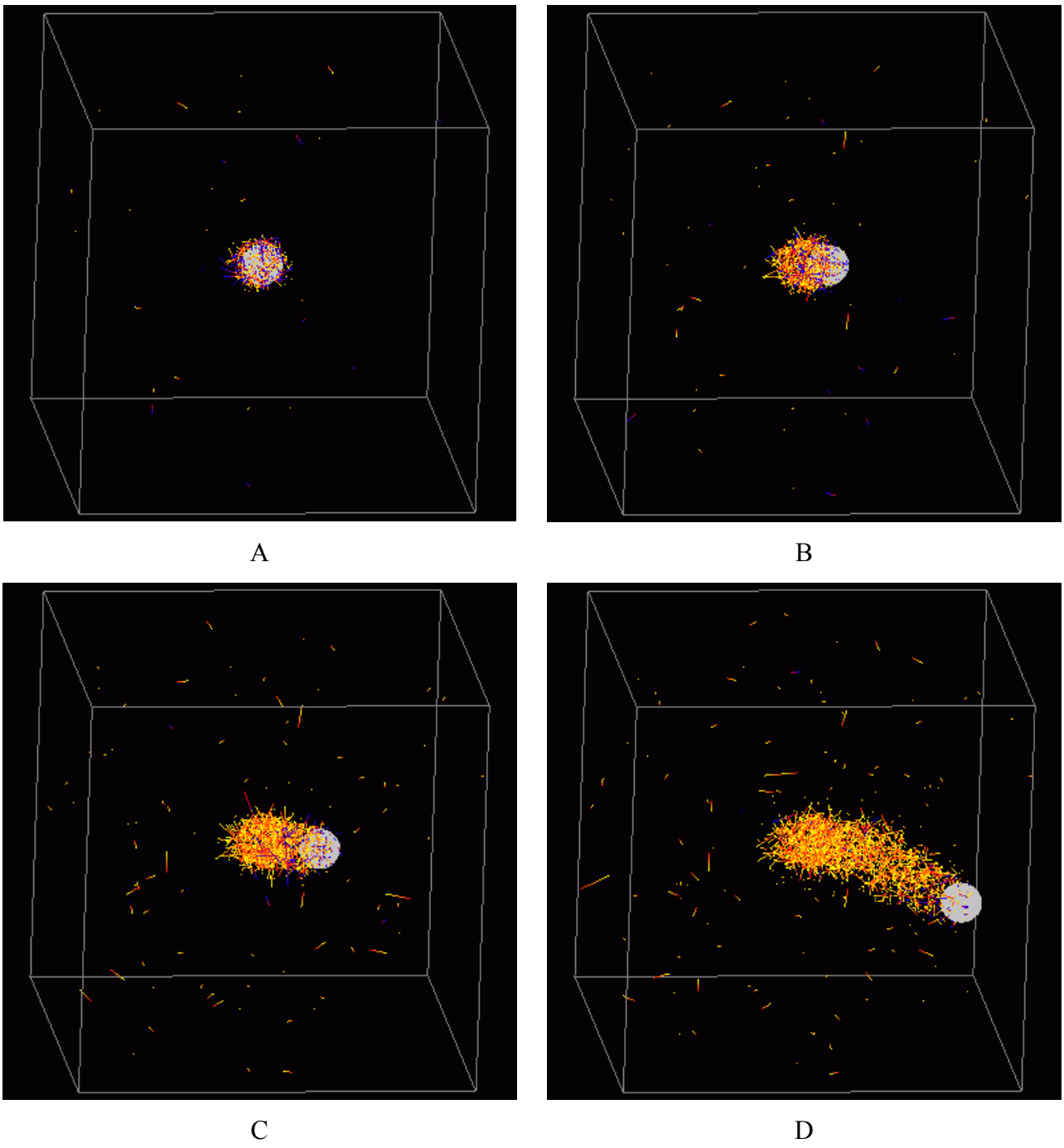

Fig. 12. Time evolution of the bead-containing system:

A – approximately 1 s after simulation, B – 3 s, C – 8 s, D – 20 s.

9. Diffusion-related models

9.1. Diffusion of monomers: theory

The study of the diffusion in a water-protein mixture was performed to answer the question about the uniform distribution of proteins in the simulated volume during biochemical reactions. The Monte Carlo based simulation approach was used. Consider the Cartesian coordinates and a cube, representing the simulated volume, with the center located in the origin of the coordinate system. The motion of molecules can be described using Ermak and McCammon algorithm (Ermak and McCammon, 1978). In this algorithm the change of each molecule's coordinates is a random value with Gaussian distribution

$$f(x)\frac{1}{\sqrt{2\pi}\sigma}\exp\left[-\frac{(x-m)^2}{2\sigma^2}\right], \quad -\infty \le x \le \infty, \tag{16}$$

with the following parameters:

- mean m=0;
- standard deviation $\sigma = \sqrt{6D\Delta t}$, where D – diffusion coefficient, Δt – time step

To estimate the diffusion coefficient, the Stocks-Einstein equation can be used, which describes the movements of a spherical body in a viscous incompressible liquid

$$D = \frac{kT}{6\pi\eta R_0}, \tag{17}$$

where R_0 is the radius of the body, η – dynamical viscosity of the liquid, k – Boltzman's constant, T – temperature of the liquid.

If should be mentioned, that application of the macro-parameters and lows to characterization of the motility of micro-objects leads to approximated results. Sometimes for better estimation of the experimental results the value 6 in the Eq. 17 can be replaced by 4. Moreover, usually it is assumed, that the micro-viscosity of liquids is lower then their macro-viscosity. Despite these empirical estimations, it is known that Stocks-Einstein equation gives correct (in the terms of orders) approximation of the real diffusion coefficient.

9.2. Diffusion of monomers: program and numerical experiments

The Monte Carlo model for the diffusion of monomers was realized as a software tool DiffusionSpeed. It is able to simulate the diffusion of several molecular species, having different

diffusion coefficients. During simulation the smaller volume *v*, located in the center of the considered volume *V*, is emptied at time $t = 0$. After that the Ermak-McCammon algorithms is utilized to recalculate positions of proteins, and the ingrowths of protein concentration in *v* is tracked and depicted on a plot.

Several numerical experiments have been performed on the molecules with the sizes close to actin monomers. In Fig. 13 two examples of the diffusion behavior are presented for the case of diffusion coefficient $D = 10$ and 50 $\mu m^2/s$ (the values on the plots are given for the virtual FRAP experiment – instead of concentration, fluorescence in mentioned). From the simulation results it can be concluded that the diffusion of monomers into the μm-scale volume occurs in a few seconds. This is in a good agreement with experimental FRAP data, obtained on actin-polymerization systems.

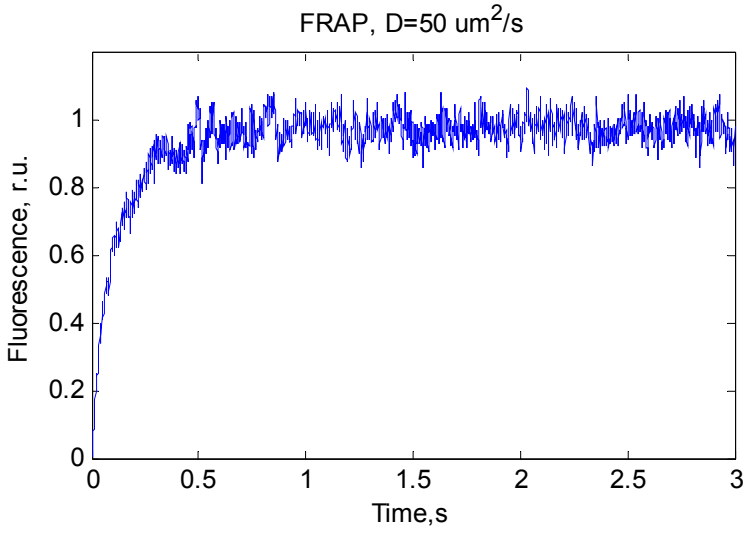

A

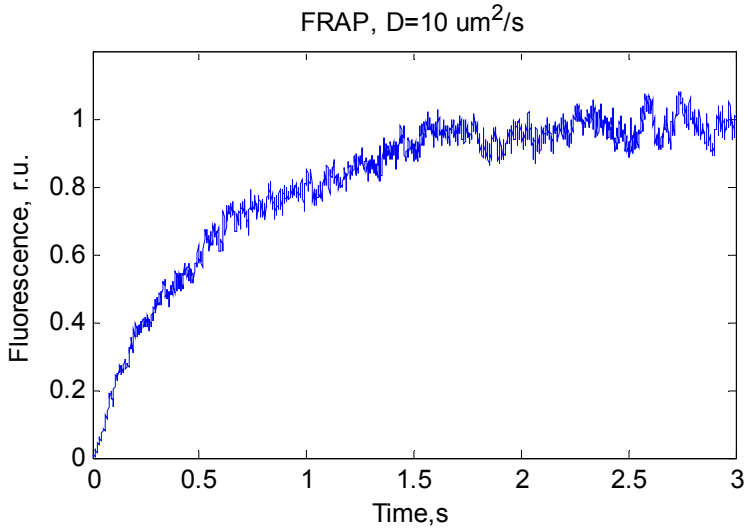

B

Fig. 13. Diffusion of proteins into a μm-scale volume in the case of D=50$\mu m^2/s$ (A) and D=1050$\mu m^2/s$ (B).

9.3. *FRAP in the presence of actin-polymerization*

The developed models of actin-polymerization can be used also for analysis of experimental FRAP data. To prove this statement, the simplified FRAP model, based on ActinSimChem, has been developed. In this model it is assumed that:

1) the simulation volume is equivalent to FRAP volume;
2) the simulation volume is surrounded by much large volume, where all fluorescent molecules are not bleached;
3) the speed of bleached monomer diffusion is high;
4) filaments are stable and do not diffuse.

The results of the FRAP simulation for two different situations (characterized by different reaction rates) are given in the Fig. 14.

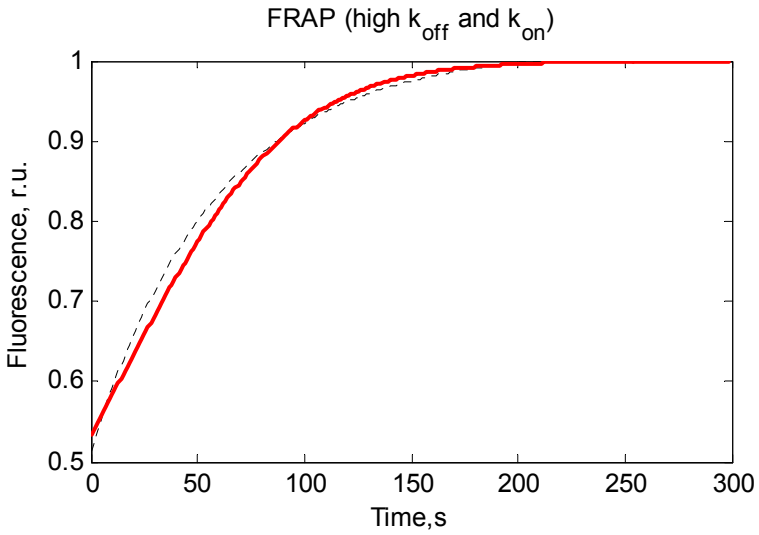

A

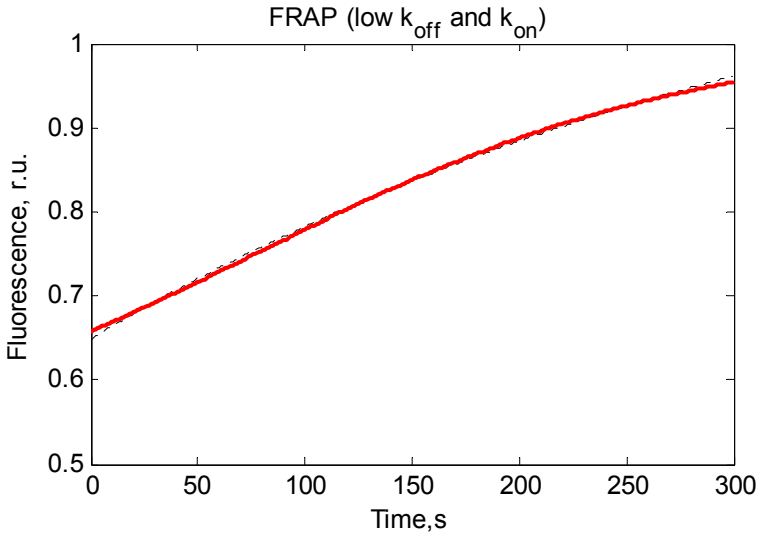

B

Fig. 14. Simulated FRAP on the volume with actin polymerization.

Plot A corresponds for the case of high association and dissociation constants, B – low.

10. Future plans

10.1. Biochemical-scale model

To study intrinsic and non-obvious properties of actin-filament systems, the aging of monomers should be taken into account. Therefore, the first step in enhancement of the molecular-scale model will be introduction of ATP and ADP containing actins. This will significantly increase the number of reactions. Moreover, it will make impossible the use of the biochemical model without structural model of actin filaments. The structural model should include precise positions of all ATP and ADP-containing actins, ATP and ADP containing barbed and pointed ends.

Moreover, in the future model it is planned to include testin (as a capper of pointed end), profilin (ATP-ADP exchanger), ActA (Arp2/3 activator) and other relevant molecular species. The preliminary list of new molecular species can be seen in the table below.

Table. 4. Complete set of relevant molecular "players"

Number	Molecule type	Abbreviation
1	G-actin with ATP	ATG
2	G-actin with ADP	ADG
3	F-actin with ATP	ATF
4	F-actin with ADP	ADF
5	Filament free barbed ends (with the last actin containing ATP)	FTB
6	Filament free barbed ends (with the last actin containing ADP)	FDB
7	Filament free pointed ends (with the last actin containing ATP)	FTP
8	Filament free pointed ends (with the last actin containing ADP)	FDP
9	Filament barbed ends from bound Arp2/3 complex	FAB
10	Arp2/3 inactive	ARP
11	Arp2/3 activated	ARA
12	Arp2/3 bound to filament	ARF
13	Free capping proteins (barbed end cappers)	CAP
14	Bound capping proteins	CAF
15	Severing protein ADF/coffilin	SEV
16	ActA – Arp2/3 activator	ACT
17	Formin (nucleator)	FOP
18	Formin in filament-bound form	FOF
19	Profilin	PRO
20	Testin (the pointed-end capper) in a free form	TEP
21	Testin (the pointed-end capper) in a filament-bound form	TEF

10.2. Mesoscale mechanical model

The enhancement of the mesoscale model will go in two directions. First – by applying new molecular species (listed in the previous section) and reactions. Second – by improving the physics of interactions and optimizing the code.

The tasks to be performed in the coming months are list below:

1) To check the work and optimize the filament-filament interactions;
2) To use more physical values for diffusion (this may lead to immediate diffusion of newly nucleated filaments from the bead surface, without producing of a shell);
3) To realize the elastic linkages between filaments and the bead.

10.3. FRAP analysis

Improved models should be used for analysis, or at least simulation of experimental FRAP data. The model for FRAP should be improved. The real structures of filaments and filament diffusion should be taken into account.

11. Summary

The literature search has been performed, providing the information about experiments and models aimed on actin-based motility study. The literature overview concerning the biophysical experiments (section 3) and models (section 4) was done. Moreover, the possible literature sources for values of relevant biophysical parameters have been found (section 5).

The published models have been analyzed and the ideas have been taken and combined in the projected simulation model briefly described in section 6. The projected model will be based on chemical reaction simulation with addition of mechanical view on actin filaments and other mesoscale bodies. It was decided to divide the model development into 3 stages: (1) development of adjustable model for biochemical reaction (protein dis-/assembly); (2) adjustment of the methodology for calculation of mechanical forces, including Brownian effects; (3) combination of chemical-reaction and force descriptions into a single mesoscale model.

The following task has been performed during first half of the project time.

- Literature studied.
- Team assembled (Nazarov, Barsukov, Ivashkevich, Golovaty, Apanasovich).
- The model for simplified reactions (8 molecular types, 6 reactions) has been developed and tested via differential equations.
- The 3D model of propelling bead has been built. Spatial representation of filaments and physical repulsion interactions has been considered.
- The model for FRAP (simplified reactions)
- The Monte Carlo diffusion model was developed.

The overviewed results are given in details in the following sections. All up-to-date sources, executable files and documents can be found at http://actinsim.nm.ru

12. References

Alberts, J. B., and Odell, G. M. (2004). In silico reconstitution of Listeria propulsion exhibits nano-saltation. PLoS Biol *2*, e412.

Atilgan, E., Wirtz, D., and Sun, S. X. (2006). Mechanics and dynamics of actin-driven thin membrane protrusions. Biophys J *90*, 65-76.

Bartles, J. R., Zheng, L., Li, A., Wierda, A., and Chen, B. (1998). Small espin: a third actin-bundling protein and potential forked protein ortholog in brush border microvilli. J Cell Biol *143*, 107-119.

Bernheim-Groswasser, A., Wiesner, S., Golsteyn, R. M., Carlier, M. F., and Sykes, C. (2002). The dynamics of actin-based motility depend on surface parameters. Nature *417*, 308-311.

Berro, J., and Martiel, J. L. (2005). In silico model for actin filament assembly based on molecule population dynamics, Paper presented at: FEBS/ESF Workshop on Integrated Approaches in Cytoskeleton Research.

Brieher, W. M., Coughlin, M., and Mitchison, T. J. (2004). Fascin-mediated propulsion of Listeria monocytogenes independent of frequent nucleation by the Arp2/3 complex. J Cell Biol *165*, 233-242.

Cameron, L. A., Footer, M. J., van Oudenaarden, A., and Theriot, J. A. (1999). Motility of ActA protein-coated microspheres driven by actin polymerization. Proc Natl Acad Sci U S A *96*, 4908-4913.

Cameron, L. A., Robbins, J. R., Footer, M. J., and Theriot, J. A. (2004). Biophysical parameters influence actin-based movement, trajectory, and initiation in a cell-free system. Mol Biol Cell *15*, 2312-2323.

Carlier, M. F., Wiesner, S., Le Clainche, C., and Pantaloni, D. (2003). Actin-based motility as a self-organized system: mechanism and reconstitution in vitro. C R Biol *326*, 161-170.

Carlsson, A. E. (2006). Stimulation of actin polymerization by filament severing. Biophys J *90*, 413-422.

DesMarais, V., Ghosh, M., Eddy, R., and Condeelis, J. (2005). Cofilin takes the lead. J Cell Sci *118*, 19-26.

Edelstein-Keshet, L., and Ermentrout, G. B. (1998). Models for the length distributions of actin filaments: I. Simple polymerization and fragmentation. Bull Math Biol *60*, 449-475.

Ermak, D. L., and McCammon, J. A. (1978). Brownian dynamics with hydrodynamic interactions. J Chem Phys *69*, 1352-1360.

Ermentrout, G. B., and Edelstein-Keshet, L. (1998). Models for the length distributions of actin filaments: II. Polymerization and fragmentation by gelsolin acting together. Bull Math Biol *60*, 477-503.

Gerbal, F., Chaikin, P., Rabin, Y., and Prost, J. (2000). An elastic analysis of Listeria monocytogenes propulsion. Biophys J *79*, 2259-2275.

Giardini, P. A., Fletcher, D. A., and Theriot, J. A. (2003). Compression forces generated by actin comet tails on lipid vesicles. Proc Natl Acad Sci U S A *100*, 6493-6498.

Giganti, A., Plastino, J., Janji, B., Van Troys, M., Lentz, D., Ampe, C., Sykes, C., and Friederich, E. (2005). Actin-filament cross-linking protein T-plastin increases Arp2/3-mediated actin-based movement. J Cell Sci *118*, 1255-1265.

Gillespie, D. T. (1977). Exact stochastic simulation of coupled chemical reactions. J Phys Chem *81*, 2340-2361.

Helfer, E., Panine, P., Carlier, M. F., and Davidson, P. (2005). The interplay between viscoelastic and thermodynamic properties determines the birefringence of F-actin gels. Biophys J *89*, 543-553.

Higgs, H. N., and Pollard, T. D. (1999). Regulation of actin polymerization by Arp2/3 complex and WASp/Scar proteins. J Biol Chem *274*, 32531-32534.

Higgs, H. N., and Pollard, T. D. (2001). Regulation of actin filament network formation through ARP2/3 complex: activation by a diverse array of proteins. Annu Rev Biochem *70*, 649-676.

Janji, B., Giganti, A., De Corte, V., Catillon, M., Bruyneel, E., Lentz, D., Plastino, J., Gettemans, J., and Friederich, E. (2006). Phosphorylation on Ser5 increases the F-actin-binding activity of L-plastin and promotes its targeting to sites of actin assembly in cells. J Cell Sci *119*, 1947-1960.

Kovar, D. R. (2006). Molecular details of formin-mediated actin assembly. Curr Opin Cell Biol *18*, 11-17.

Loomis, P. A., Zheng, L., Sekerkova, G., Changyaleket, B., Mugnaini, E., and Bartles, J. R. (2003). Espin cross-links cause the elongation of microvillus-type parallel actin bundles in vivo. J Cell Biol *163*, 1045-1055.

Marcy, Y., Prost, J., Carlier, M. F., and Sykes, C. (2004). Forces generated during actin-based propulsion: a direct measurement by micromanipulation. Proc Natl Acad Sci U S A *101*, 5992-5997.

McGrath, J. L., Osborn, E. A., Tardy, Y. S., Dewey, C. F., Jr., and Hartwig, J. H. (2000). Regulation of the actin cycle in vivo by actin filament severing. Proc Natl Acad Sci U S A *97*, 6532-6537.

Ming, D., Kong, Y., Wu, Y., and Ma, J. (2003). Simulation of F-actin filaments of several microns. Biophys J *85*, 27-35.

Mogilner, A., and Edelstein-Keshet, L. (2002). Regulation of actin dynamics in rapidly moving cells: a quantitative analysis. Biophys J *83*, 1237-1258.

Mogilner, A., and Oster, G. (2003). Force generation by actin polymerization II: the elastic ratchet and tethered filaments. Biophys J *84*, 1591-1605.

Mogilner, A., and Rubinstein, B. (2005). The physics of filopodial protrusion. Biophys J *89*, 782-795.

Noireaux, V., Golsteyn, R. M., Friederich, E., Prost, J., Antony, C., Louvard, D., and Sykes, C. (2000). Growing an actin gel on spherical surfaces. Biophys J *78*, 1643-1654.

Plastino, J., Olivier, S., and Sykes, C. (2004). Actin filaments align into hollow comets for rapid VASP-mediated propulsion. Curr Biol *14*, 1766-1771.

Pollard, T. D., and Beltzner, C. C. (2002). Structure and function of the Arp2/3 complex. Curr Opin Struct Biol *12*, 768-774.

Pollard, T. D., and Borisy, G. G. (2003). Cellular motility driven by assembly and disassembly of actin filaments. Cell *112*, 453-465.

Romero, S., Le Clainche, C., Didry, D., Egile, C., Pantaloni, D., and Carlier, M. F. (2004). Formin is a processive motor that requires profilin to accelerate actin assembly and associated ATP hydrolysis. Cell *119*, 419-429.

Samarin, S., Romero, S., Kocks, C., Didry, D., Pantaloni, D., and Carlier, M. F. (2003). How VASP enhances actin-based motility. J Cell Biol *163*, 131-142.

Sept, D., and McCammon, J. A. (2001). Thermodynamics and kinetics of actin filament nucleation. Biophys J *81*, 667-674.

Sirotkin, V., Beltzner, C. C., Marchand, J. B., and Pollard, T. D. (2005). Interactions of WASp, myosin-I, and verprolin with Arp2/3 complex during actin patch assembly in fission yeast. J Cell Biol *170*, 637-648.

Thoumine, O., Lambert, M., Mege, R. M., and Choquet, D. (2006). Regulation of N-cadherin dynamics at neuronal contacts by ligand binding and cytoskeletal coupling. Mol Biol Cell *17*, 862-875.

Tracqui, P., Promayon, E., Amar, P., Huc, N., Norris, V., and Martiel, J. L. (2004). Emergent features of cell structural dynamics: a review of models based on tensegrity and nonlinear oscillations.

Tseng, Y., Schafer, B. W., Almo, S. C., and Wirtz, D. (2002). Functional synergy of actin filament cross-linking proteins. J Biol Chem *277*, 25609-25616.

Upadhyaya, A., Chabot, J. R., Andreeva, A., Samadani, A., and van Oudenaarden, A. (2003). Probing polymerization forces by using actin-propelled lipid vesicles. Proc Natl Acad Sci U S A *100*, 4521-4526.

van der Gucht, J., Paluch, E., Plastino, J., and Sykes, C. (2005). Stress release drives symmetry breaking for actin-based movement. Proc Natl Acad Sci U S A *102*, 7847-7852.

van Oudenaarden, A., and Theriot, J. A. (1999). Cooperative symmetry-breaking by actin polymerization in a model for cell motility. Nat Cell Biol *1*, 493-499.

Vignjevic, D., Yarar, D., Welch, M. D., Peloquin, J., Svitkina, T., and Borisy, G. G. (2003). Formation of filopodia-like bundles in vitro from a dendritic network. J Cell Biol *160*, 951-962.

Zicha, D., Dobbie, I. M., Holt, M. R., Monypenny, J., Soong, D. Y., Gray, C., and Dunn, G. A. (2003). Rapid actin transport during cell protrusion. Science *300*, 142-145.